THE JOURNAL OF PHYSICAL CHEMISTRY C
A JOURNAL OF THE AMERICAN CHEMICAL SOCIETY

pubs.acs.org/JPCC

Article

Theoretical Insights into Metal-Catalyzed Associative Electrochemical Conversion of NO_x in Aqueous Solution

Published as part of The Journal of Physical Chemistry C special issue "Francesc Illas and Gianfranco Pacchioni Festschrift".

Pilar Carro, Raúl Quesada-Cabrera, José Miguel Doña-Rodríguez, and Luis Miguel Azofra*

Cite This: https://doi.org/10.1021/acs.jpcc.4c08529

Read Online

ACCESS | Metrics & More | Article Recommendations | Supporting Information

ABSTRACT: The present study investigated a mechanistic analysis of the electrocatalytic reduction of nitrogen oxides (NO_x; x = 1, 2) into ammonia (NH_3) on flat surfaces of selected middle-to-late *d*-block metals, viz., Fe, Co, Ni, Cu, Zn, Mo, Ru, Rh, Pd, Ag, Os, Ir, Pt, and Au. Our DFT calculations were carried out in aqueous solution via an implicit solvation model, also providing insights into the impact of the pH on the reduction process. At a mechanistic level, the first four reductive steps entail the O-hydrogenation from NO_x via the path $*NO_2 \rightarrow *NO_2H \rightarrow *NO\ (+H_2O) \rightarrow *NOH \rightarrow *N\ (+H_2O)$. Subsequently, the as-generated N adatoms are hydrogenated to form ammonia following the path $*N \rightarrow *NH \rightarrow *NH_2 \rightarrow *NH_3$. In this mechanism, the conversions of $*NO_2$ into $*NO_2H$ and *NO into *NOH were generally identified as the rate-determining steps. In addition, binding of NO_2 and NO has been computed to be stronger than NH_3 adsorption in most cases, which prevents ammonia poisoning on the metal surfaces. Finally, our results show the existence of periodic behaviors in all of the modeled stages of the NO_x reduction mechanism, revealing strong correlation among the free energies involved in the steps *NO to *NOH and *NOH or *N to $*NH_x$ at different levels of hydrogenation.

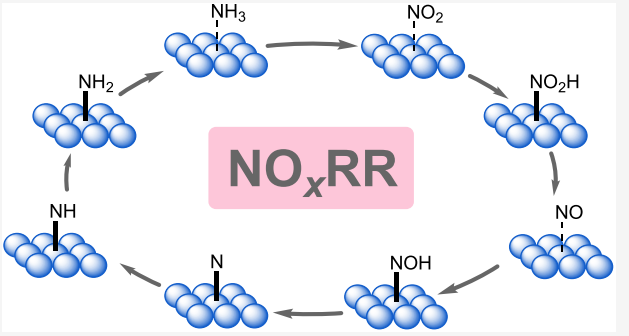

INTRODUCTION

In recent years, the electrochemical production of green ammonia (eNH_3) from reduction of air-sourced nitrogen (N_2) has been the focus of intense research in the field of N_2 fixation.[1,2] This prominent technology has not been exempted from controversy around the nitrogen source, questioning whether the NH_3 generated was due to spurious nitrogen sources such as nitrogen oxides (NO_x).[3,4] This controversy has been incited by inconsistent results in the literature, mainly due to the inadequate use of quantitative determination methods. In this sense, consolidated research groups in the field have independently published a series of protocols advocating toward thorough quantification procedures[4−6] to establish unequivocal routes to eNH_3 from the reduction of N_2 alone and not from other sources.

Previous work by some of the current authors included a comprehensive DFT study showing the preferential reduction of NO_x (NO_xRR) over N_2 reduction (NRR)[7] on *d*-block metal electrodes under reducing conditions, attributing the formation of NH_3 to the presence of ubiquitous nitrogen-containing contaminants in many reported cases.

Direct N_2-into-NH_3 conversion under mild conditions is indeed a challenging process, supported by a very limited number of robust electrocatalysts. Alternatively, some authors have now paid attention to the NO_xRR conversion as a potential route to a large-scale production of eNH_3. Long et al.,[8] for instance, used a copper foam to produce NH_3 from nitric oxide (NO) gas, reporting production rates of 517.1 μmol cm^{-2} h^{-1} at −0.9 V vs. RHE and a Faradaic efficiency (FE) of 93.5% over a period of 100 h. In the last years, numerous materials, including *d*-block metals such as Fe,[9] Co,[9,10] Ni,[9] Ru,[11] Pd,[9] Ag,[9] or Pt,[9] transition metal alloys,[12] single-atom-decorated materials on metals,[13,14] MoS_2,[15,16] or MoO_3,[17−20] and *p*-block metals such as Bi,[21] metal oxides,[22,23] carbides,[24,25] sulfides,[26] phosphides,[27] and many others, have demonstrated ability to carry out the NO_xRR process (predominantly NORR).

The role of ammonia as a primary consumer good, as the main precursor to most synthetic fertilizers[28] and as a promising energy vector,[29,30] is indisputable. A question remains on the feasibility of eNH_3 production at medium or large scale using NO_x as a raw material. In any case, the high selectivity and

Received: December 17, 2024
Revised: March 7, 2025
Accepted: April 7, 2025

Downloaded via UNIV LAS PALMAS GRAN CANARIA on April 21, 2025 at 14:22:30 (UTC).
See https://pubs.acs.org/sharingguidelines for options on how to legitimately share published articles.

ACS Publications
© XXXX American Chemical Society

efficiency rates reported for a widespread number of available electrocatalysts advocate for a promising alternative route to NO_x removal methods from air pollution.[31]

In the present study, a series of *d*-block metals were investigated to model the interactions of the different intermediate states during NO_xRR into NH_3 in aqueous solution. These calculations used the flat surfaces (110), (111), and (0001) of body-centered cubic (Fe, Mo), face-centered cubic (Ni, Cu, Rh, Pd, Ag, Ir, Pt, Au), and hexagonal-close packing (Co, Zn, Ru, and Os) metals, respectively (Scheme 1). Correlation among crystal structures, corresponding free energies, and physicochemical behavior indicated periodic trends across these electrocatalysts.

Scheme 1. Selected *d*-Block Metals Used in This Study as Electrocatalysts for NO_x Reduction (NO_xRR) into NH_3 in Aqueous Solution[a]

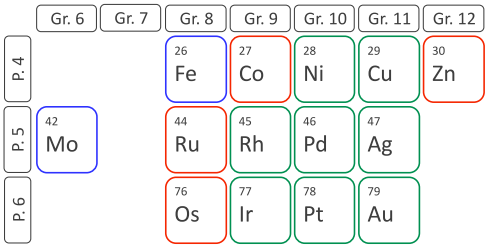

[a]Box outlines refer to the type of atomic packing, namely, bcc (blue line), fcc (green line), and hcp (red line), respectively.

These results provide key insight into the mechanism of NO_xRR toward eNH_3 production, as well as better understanding of the electrocatalytic capabilities of transition metals in the nitrogen chemistry. The promising catalytic indicators reported in this work also open opportunities toward an alternative electrochemical route for the abatement of atmospheric NO_x.[31]

COMPUTATIONAL METHODS

The mechanism for NO_x conversion into NH_3 catalyzed by a series of *d*-block metals was studied by DFT through the generalized gradient approximation (GGA). To this end, the revised Perdew–Burke–Ernzerhof (RPBE) functional with Pade approximation[32] was used with a plane-wave cutoff energy of 400 eV. Bulk materials were fully optimized with very tight convergence criteria, specifically, energy and force convergence limits equal to 10^{-5} eV/atom and |0.001| eV/Å, respectively. The Brillouin zone (periodic boundary conditions) was sampled via the Monkhorst–Pack scheme,[33] increasing the number of *k*-points up to reach electronic energy differences less than |0.01| eV. Once the bulk structures were optimized, (110), (111), (0001) flat surfaces were built for bcc (Fe, Mo), fcc (Ag, Au, Cu, Ir, Ni, Pd, Pt, Rh), and hcp (Co, Os, Ru, Zn) metals, respectively, reoptimizing with a vacuum width of 15 Å to avoid interactions between periodic slabs. For the specific cases of Fe, Ni, and Co, spin-polarized calculations were performed. All slabs were composed of 36 atoms, in four layers of (3 × 3) unit cell. The modeling of such clean surfaces, as well as the intermediate states from NO_x adsorption to NH_3 desorption upon conversion, were carried out using energy and force convergence limits of 10^{-4} eV/atom and |0.01| eV/Å, respectively, and 3 × 3 × 1 *k*-points. In all cases, explicit energy dispersion correction terms were included through the D3 method with the standard parameters programmed by Grimme and co-workers,[34,35] also incorporating solvent effects (aqueous solution) via VASPsol kit.[36,37] Further details about the computational methodology can be found in the Supporting Information (SI). All optimization and vibrational frequency calculations were performed using the Vienna Ab Initio Simulation Package (VASP, version 5.4.4).[38−41]

RESULTS AND DISCUSSION

The NO_x reduction mechanism, starting from its most oxidized form (NO_2), involved the addition of seven H^+/e^- pairs in successive elementary reactions. In the first stage, it involved the O-hydrogenation from NO_x, with concomitant formation of water $*NO_2 \rightarrow *NO_2H \rightarrow *NO\ (+H_2O) \rightarrow *NOH \rightarrow *N\ (+H_2O)$, followed by the sequential hydrogenation of N adatoms to form NH_3: $*N \rightarrow *NH \rightarrow *NH_2 \rightarrow *NH_3$. This mechanistic pathway (Figure 1) follows a Heyrovsky-type

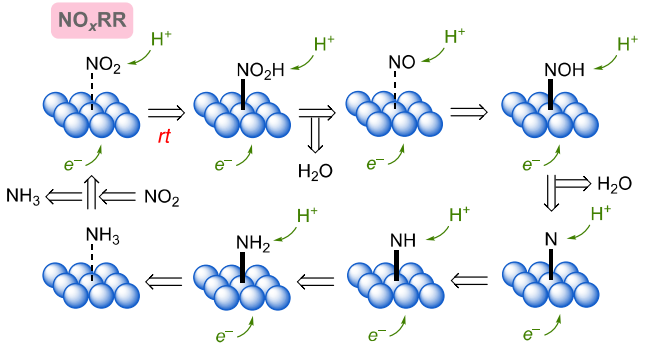

Figure 1. Schematic of the reaction mechanism for the reduction of NO_x (NO_xRR) into NH_3 at room temperature (*rt*).

associative route (O-side),[42] where NO_x molecules (either NO_2 or NO) are first adsorbed on the metal surface and subsequently hydrogenated upon addition of successive H^+/e^- pairs.

The choice of this mechanistic route is not arbitrary and is supported by binding free energy (ΔG_b) calculations (Table S2). For all selected metals, both NO_2 and NO adsorption present ΔG_b values of greater stability than those of the formation of H adatoms (*H) as a result of the reduction of protons, which could be produced through the competitive hydrogen evolution reaction (HER), $* + H^+ + e^- \rightarrow *H$. In most cases, both NO_2 and NO showed a strong Lewis base behavior toward the series of metals studied here. Specifically, the formation of $*NO_2$ showed spontaneous ΔG_b values, as it was also the case for the formation of *NO, except for d^9 Ag and Au, and d^{10} Zn metals, with slightly endergonic ΔG_b(*NO) values. In any case, these binding free energies were higher than those necessary for the formation of *H, which implied greater selectivity on the part of NO_x to compete for the Lewis acid binding sites on metal surfaces. These results were observed both at neutral pH (pH 7), where H^+ reduction is less favored with respect to pH-independent NO_x adsorptions, and under acidic conditions (pH 0).

One of the general aspects of the NO_xRR catalyzed by this series of *d*-block metals is that, during the first four reductive steps that constitute O-hydrogenation from NO_x stage, the first and third (odd) additions of H^+/e^- pairs were endergonic while the second and fourth (even) additions were exergonic. Figure 2 gathers the free energy profiles, grouped by period, obtained during the modeling of the NO_x reduction catalyzed for all of

https://doi.org/10.1021/acs.jpcc.4c08529
J. Phys. Chem. C XXXX, XXX, XXX−XXX

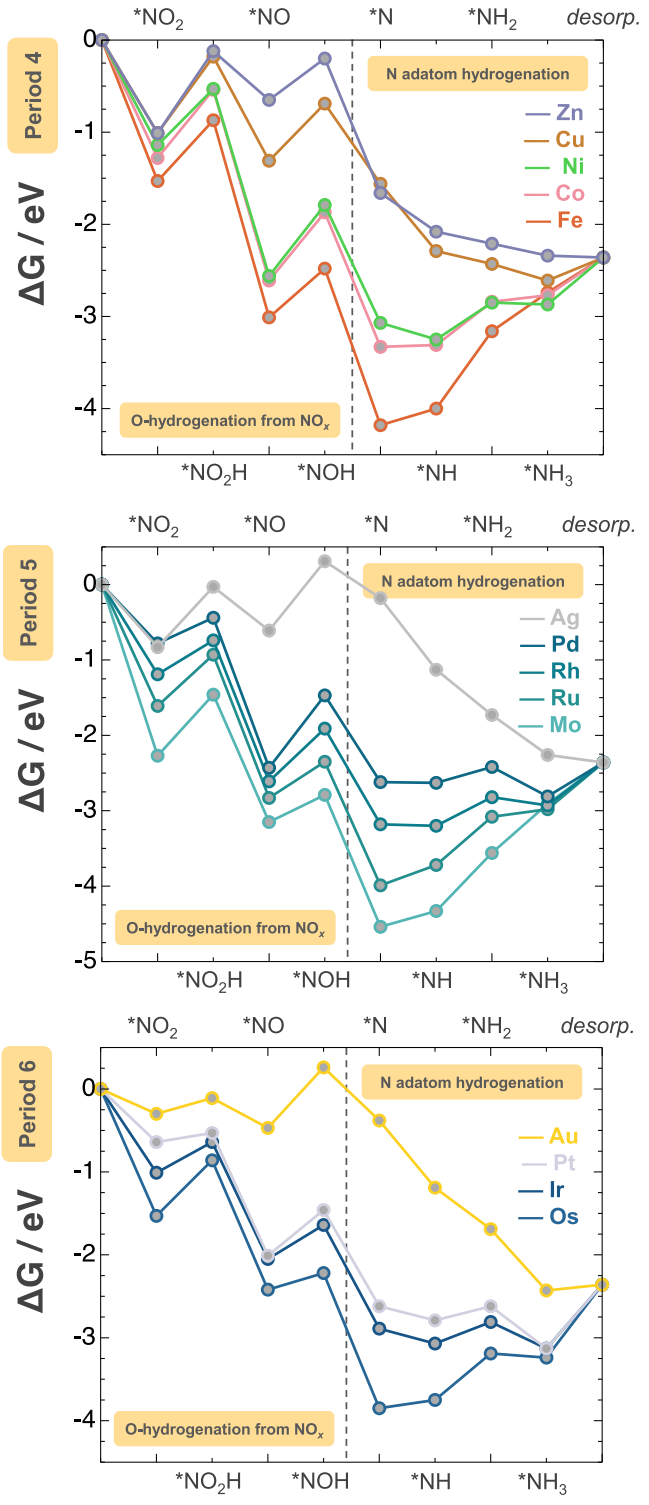

Figure 2. Free energy (ΔG) profiles (in eV) for the electrochemical NO_x reduction (NO_xRR) catalyzed by selected period-4 (top), period-5 (center), and period-6 (bottom) *d*-block metals. All results are shown at a neutral pH (pH 7) with no applied bias ($U = 0$) in aqueous solution.

these metals. Note that both $*NO_2H$/*NO and *NOH/*N conversions are downhill steps in the potential energy surface (PES), while $*NO_2$/$*NO_2H$ and *NO/*NOH conversions are uphill steps. This trend was observed in all cases at neutral pH (pH 7) as shown in Figure 2. Interestingly, the successive hydrogenation steps of the N adatom, respectively, into *NH, $*NH_2$, and $*NH_3$, presented an energy profile that depended on the nature of the electrocatalyst, rather than the step in which the H^+/e^- pair was added. In this second stage, periodic behavior was observed where middle transition metals showed high stabilization of the N adatom (*N) and an uphill sequence following *NH → $*NH_2$ → $*NH_3$ hydrogenations, whereas late transition metals presented decreasing stabilization of *N and downhill free energies for such hydrogenations. The trend of endergonic steps for the hydrogenation of *N and $*NH_x$ species was more pronounced in middle transitions metals such as Mo, Fe, Ru, and Co, decreasing along the period until the change in trend as we approached to late transitions metals, e.g., Zn, Ag, and Au.

Further insight into the energies and structures of the reaction intermediates of the NO_xRR process is shown in Figure 3, including the optimized structures for all states of the process. A common aspect for all selected metals is the spontaneous adsorption of NO_2 via chelation with both of their O atoms. Although these are arranged by packing (first bcc, followed by fcc, and last bcc), it can be observed that, for a given period, there was a decrease in binding free energy with respect to the atomic number. For instance, the ΔG_b values along the fourth-period metals Fe, Co, Ni, Cu, and Zn were, respectively, −1.53, −1.28, −1.14, −1.01, and − 1.01 eV. This trend was also observed for fifth-period metals Mo, Ru, Rh, Pd, and Ag, with −2.27, −1.61, −1.19, −0.78, and −0.83 eV, respectively, and for sixth-period metals Os, Ir, Pt, and Au, with −1.53, −1.01, −0.64, and −0.30 eV, respectively.

A distinguishing feature was the type of adsorption of NO_2H species as a result of the first hydrogenation of $*NO_2$ whereby, the more electropositive metals, such as Mo, Fe, Ru, and Os, showed NO_2H species anchored to the metal surface by means of both N and nonhydrogenated O atoms. That contrasted with the rest of the metals, viz., Co, Ni, Cu, Zn, Rh, Pd, Ag, Ir, and Pt, in which the NO_2H species bound onto the surface via N alone. In the exceptional case of Au, the least electropositive metal of this list, the NO_2H species did not bind to the surface. On the other hand, both *NO and *NOH adsorbates bound via N binding in all cases, while adsorbates *N and $*NH_x$ via three, two, or one metal−N bond, respectively, for *NH, $*NH_2$, or $*NH_3$, without finding any divergence among the metals studied.

Regarding ammonia desorption, we obtained positive free energies, i.e., where NH_3 adheres with spontaneous interactions, thus requiring the application of energy for the release of NH_3, except in the most electropositive metals, Ag and Zn. Nevertheless, all of these energies are lower than those released by adsorption of NO_2 and NO, with the exception of Pt for the case of NO_2 and Zn and Au for the case of NO, indicating a preference for these surfaces to host NO_2 and NO species in favor of NH_3 poisoning. It is also worth mentioning that NO adsorption is usually stronger than NO_2 adsorption, reversing this trend for the less electropositive metals Cu, Zn, Ag, and Au.

In general, it was found that the limiting steps in the NO_xRR were due to the hydrogenation of either $*NO_2$ into $*NO_2H$ or *NO into *NOH, with the only exception of Fe, where the hydrogenation step of *NH into $*NH_2$ (0.84 eV) was slightly higher than the second more endergonic step, $*NO_2$ into $*NO_2H$ (0.66 eV). These data are highlighted in Figure 3. Thus, it was found that the rate-determining steps (RDS) for Ag, Au, Ir, Ni, Pd, Pt, Rh, and Co metals were due to NO hydrogenation into *NOH, with corresponding relative free energies ($\Delta\Delta G$) of 0.92, 0.73, 0.41, 0.77, 0.96, 0.55, 0.70, and 0.74 eV, respectively. In contrast, for Mo, Cu, Os, Ru, and Zn metals, the RDS values

https://doi.org/10.1021/acs.jpcc.4c08529
J. Phys. Chem. C XXXX, XXX, XXX−XXX

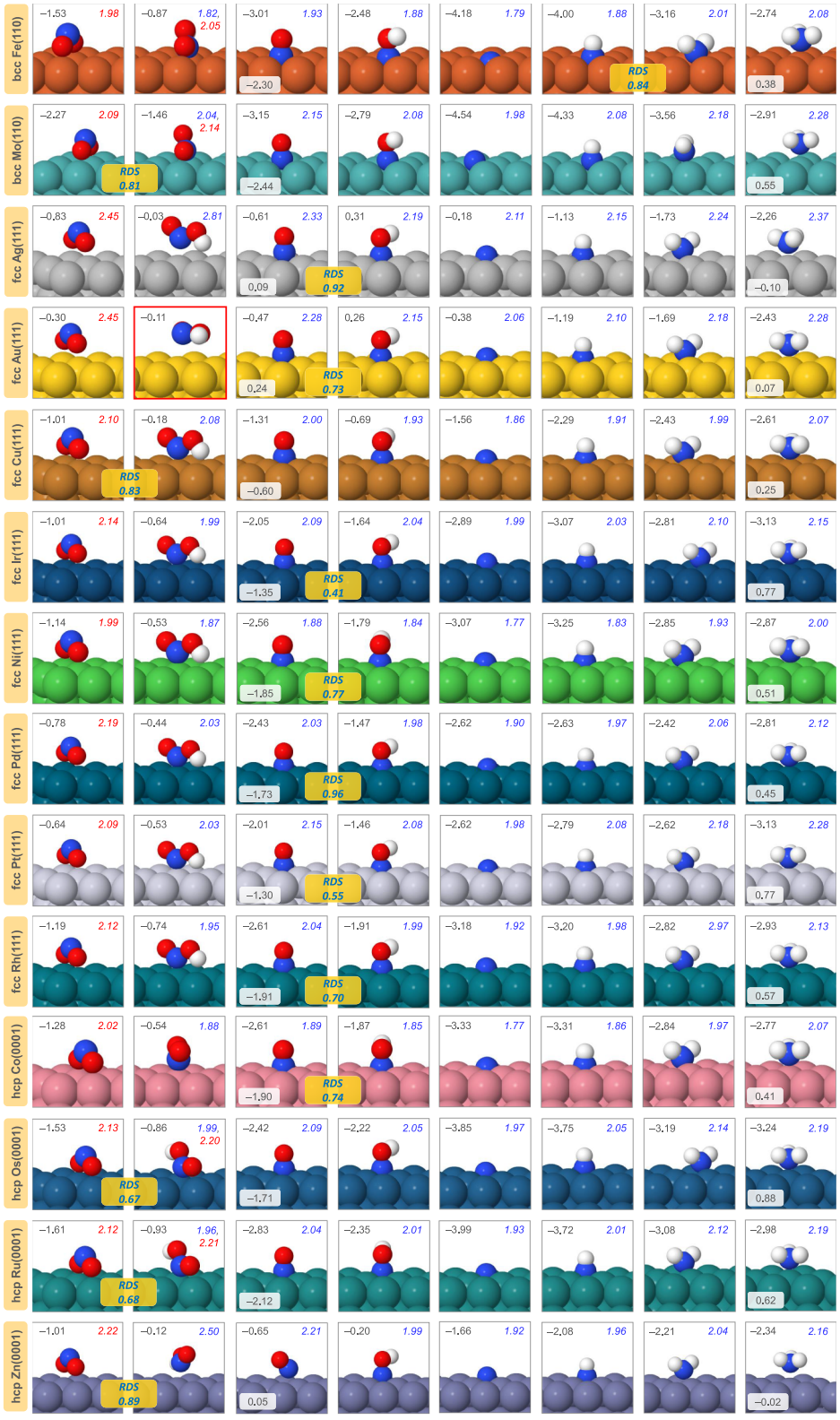

Figure 3. Optimized structures obtained during the modeling of NO_x reduction (NO_xRR) into NH_3 catalyzed by selected *d*-block metals. Free energy values (ΔG, in eV) are given in the top row (gray) together with the shortest O···M (red) and N···M (blue) distances (in Å), referring "M" to the metal. Rate-determining steps (RDS, in eV) are highlighted in yellow boxes. Binding free energies, in eV, for NO adsorption and NH_3 desorption are also indicated in white boxes. These values correspond to neutral pH conditions (pH 7) with no applied bias (U = 0 V) and are modeled in aqueous solution. Notes: H atoms in the $*NO_2H$ states for Fe, Co, and Mo are hidden, pointing behind the plane. Furthermore, the $*N_2OH$ state for Au is highlighted in red, as no direct interaction between this substrate and the metal surface is described.

were due to NO_2 hydrogenation into $*NO_2H$, with $\Delta\Delta G$ values of 0.81, 0.83, 0.67, 0.68, and 0.89 eV, in each case. These steps of greater free energy contribution are associated with maximum overpotentials, η, within the general redox reaction since η =

https://doi.org/10.1021/acs.jpcc.4c08529
J. Phys. Chem. C XXXX, XXX, XXX−XXX

Table 1. Summary of Most Important Free Energy Quantities (in eV) Obtained in the Modeling of NO_x Reduction (NO_xRR) for Selected Metals

metal	limiting step	$\Delta\Delta G_{max}$ (pH 0)	$\Delta\Delta G_{max}$ (pH 7)	ΔG_b (*NO_2)	ΔG_b (*NO)	ΔG_d (*NH_3)	ΔG(*H) (pH 0)	ΔG(*H) (pH 7)
bcc Fe(110)	*NH to *NH_2	0.42	0.84	−1.53	−2.30	0.38	−0.61	−0.20
hcp Co(0001)	*NO to *NOH	0.32	0.74	−1.28	−1.90	0.41	−0.43	−0.02
fcc Ni(111)	*NO to *NOH	0.35	0.77	−1.14	−1.85	0.51	−0.43	−0.02
fcc Cu(111)	*NO_2 to *NO_2H	0.42	0.83	−1.01	−0.60	0.25	−0.11	0.31
hcp Zn(0001)	*NO_2 to *NO_2H	0.48	0.89	−1.01	0.05	−0.02	0.61	1.02
bcc Mo(110)	*NO_2 to *NO_2H	0.40	0.81	−2.27	−2.44	0.55	−0.59	−0.17
hcp Ru(0001)	*NO_2 to *NO_2H	0.27	0.68	−1.61	−2.12	0.62	−0.49	−0.07
fcc Rh(111)	*NO to *NOH	0.29	0.70	−1.19	−1.91	0.57	−0.39	0.02
fcc Pd(111)	*NO to *NOH	0.55	0.96	−0.78	−1.73	0.45	−0.46	−0.04
fcc Ag(111)	*NO to *NOH	0.50	0.92	−0.83	0.09	−0.10	0.33	0.74
hcp Os(0001)	*NO_2 to *NO_2H	0.26	0.67	−1.53	−1.71	0.88	−0.42	−0.01
fcc Ir(111)	*NO to *NOH	0.00	0.41	−1.01	−1.35	0.77	−0.26	0.16
fcc Pt(111)	*NO to *NOH	0.14	0.55	−0.64	−1.30	0.77	−0.34	0.07
fcc Au(111)	*NO to *NOH	0.32	0.73	−0.30	0.24	0.07	0.27	0.68

$-\Delta\Delta G_{max}/e$. Close inspection of Figure 3 suggests that both Ir and Pt metals show excellent catalytic indicators for NO_xRR, with overpotentials of only −0.41 and −0.55 V vs. NHE at neutral pH. Nevertheless, it is worth mentioning that, in general, low overpotentials were obtained for all metals of this series, with values less than 1 eV. Since our calculations also included solvent effects, these thermodynamics data are a good indicator of the electrocatalytic capability of the materials studied herein for the catalysis of the NO_xRR process in aqueous solution. Our results are in good agreement with those previously reported in the literature. For instance, Long et al.[8] calculated an energy drop of ca. 0.4 and 1.7 eV from NO(g) to *NOH and *N in NORR, respectively, which is consistent with the values obtained in this work (−0.40 and − 1.68 eV, in each case). More recently, Wang et al.[43] have computed free energies of ca. −0.7, −0.2, −2.5, and −1.8 eV for the *NO_2, *NO_2H, *NO, and *NOH steps in NO_2RR catalyzed by Cu(111), although followed by an alternating mechanism from the *NOH formation stage. Our results followed this same trend, with slight differences (−1.01, −0.59, −2.13, and −1.93 eV, respectively). A recent review by Du and co-workers[44] and references therein included data for other metals. For example, Wang et al.[10] computed a relative barrier of *ca.* 0.3 eV for the *NO into *NOH stage on Co(0001), which agrees with our value (0.32 eV). Other recent works such as that reported by Xie et al.[45] using Pd(111) do not allow comparisons with our results since the mechanism has been based on the O-type adsorption of all intermediates, a hypothesis that differs from ours.

Table 1 includes a summary of the most important free energy quantities obtained in the modeling of NO_x reduction (NO_xRR) catalyzed by the series of *d*-block metals studied herein. Specifically, maximum free energies ($\Delta\Delta G_{max}$) associated with RDS, binding NO_2 [ΔG_b(*NO_2)] and NO [ΔG_b(*NO)] free energies, NH_3 desorption [ΔG_d(*NH_3)] free energies, and formation free energies for *H [ΔG(*H)] are shown. $\Delta\Delta G_{max}$ at acidic (pH 0) and neutral (pH 7) conditions are explicitly indicated together with the associated limiting steps for such values. Binding free energies for NO_2 [* + NO_2(ac) → *NO_2] and NO [* + NO(ac) → *NO] can be directly compared with NH_3 desorption [*NH_3 → * + NH_3(ac)] and *H formation during HER. From these results, it can be concluded that (i) with the exception of Pt, the adsorption of NO_2 is stronger than the adsorption of NH_3 for all metals studied [note that ΔG_b(*NH_3) = − ΔG_d(*NH_3)], i.e., NO_2 shows greater binding stabilization, which could displace NH_3 molecules and avoid the poisoning of the surface by these species, a common problem in the reduction process of other nitrogenous species such as NRR;[46,47] (ii) this is also observed for the NO species, with the exception of Zn and Au; and (iii) in all cases, the adsorption of any of the NO_x species would be stabilized over formation of intermediate *H species under the whole range of pH conditions studied here. Thus, for the series of metals studied herein, NO_xRR appears to be a more competitive process than HER, in agreement also with recent results reported by our group.[7]

Beyond the identification of those metals with the best ability to catalyze the NO_xRR, it was also interesting to explore any potential periodic behavior across the catalytic properties of these surfaces. In particular, we wanted to understand whether there was any periodicity in the formation energies of these intermediate species and, in that case, whether there was any correlation in such periodic behaviors. Figure 4 shows a representation of $\Delta\Delta G_{max}$, gathered from Table 1, as a function of the atomic number for the selected series of *d*-block metals studied herein. A general trend was observed for a given period, where the maximum free energy required in the computed limiting steps found a minimum around group-9 metals. Motivated by the appearance of this trend, an exhaustive comparison was established among all energy indicators (Figure 5) in order to intercept more pronounced periodic behaviors

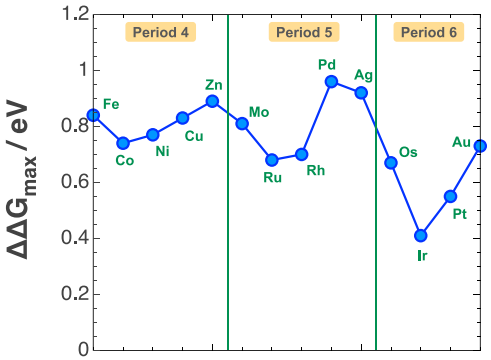

Figure 4. Representation of the maximum free energies, as $\Delta\Delta G$ in eV, computed for each metal vs. the increased atomic number for the NO_x reduction (NO_xRR) into the NH_3 mechanism at neutral pH (pH 7) and in aqueous solution when no bias (U = 0) is applied.

https://doi.org/10.1021/acs.jpcc.4c08529
J. Phys. Chem. C XXXX, XXX, XXX−XXX

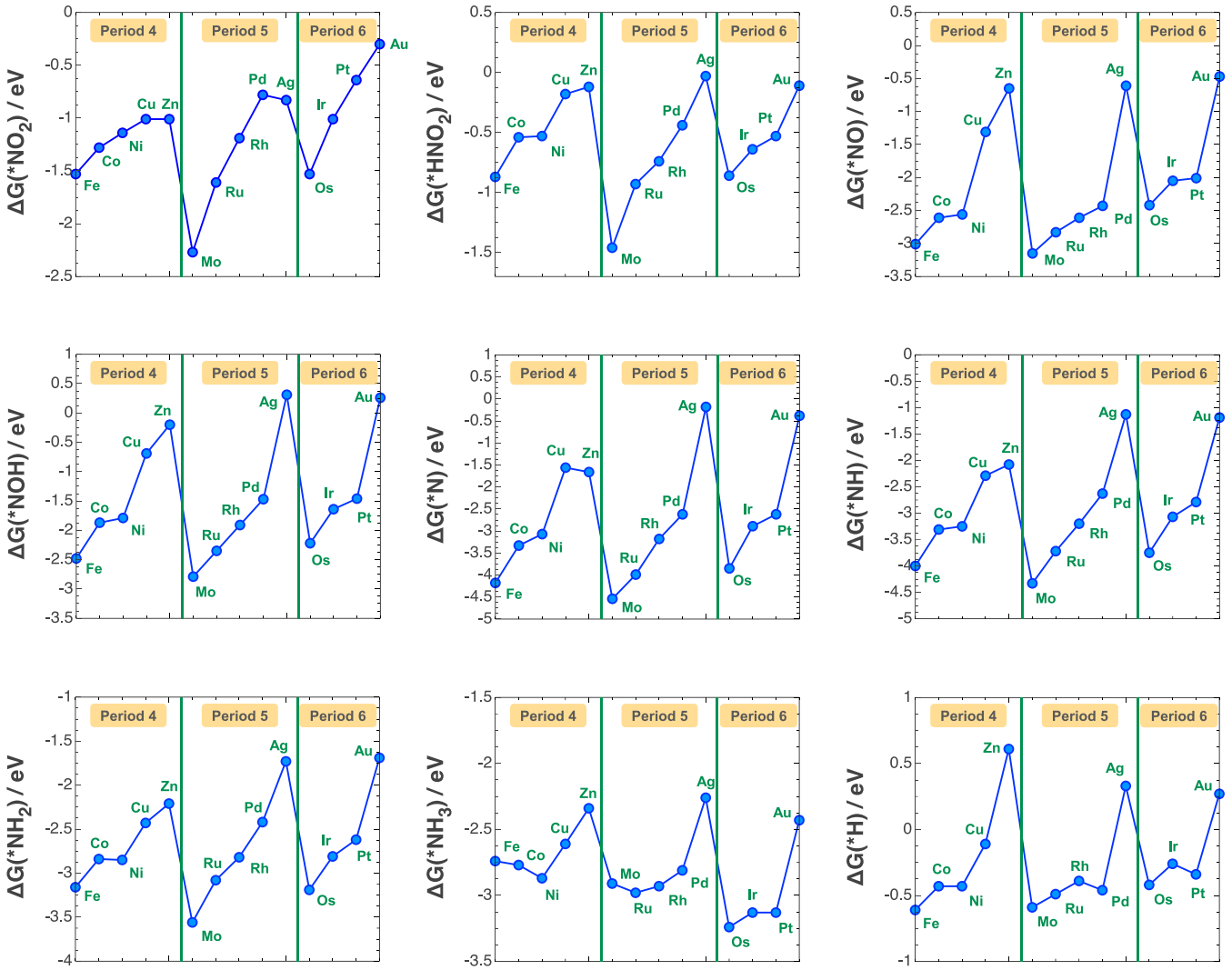

Figure 5. Representation of the free energies, ΔG in eV, corresponding to all steps during the modeling of NO_x reduction (NO_xRR) into NH_3 vs. the atomic number for the group of selected *d*-block metals studies herein. The free energy for the formation of *H as the intermediate state of HER is also presented.

exempted of fluctuations. Surprisingly, the free energies for the formation of all intermediate states, including binding estimations of NO_2 adsorption, showed an increasing trend becoming less exergonic upon increasing the atomic number. Only the formation of $*NH_3$ exhibited fluctuations in this marked trend, which has also been observed in the formation free energies of *H, as intermediate state in HER. Similar variations were otherwise obtained across the periodic profiles for *NO, *NOH, *N, and $*NH_x$ species ($x = 1, 2$). These linear correlations can be described following eqs 1−7:

$$\Delta G(^*\mathrm{NOH}) = 1.06\ \Delta G(^*\mathrm{NO}) + 0.73;\ R^2 = 0.96 \quad (1)$$

$$\Delta G(^*\mathrm{N}) = 1.33\ \Delta G(^*\mathrm{NOH}) - 0.79;\ R^2 = 0.98 \quad (2)$$

$$\Delta G(^*\mathrm{NH}) = 0.96\ \Delta G(^*\mathrm{NOH}) - 1.52;\ R^2 = 0.97 \quad (3)$$

$$\Delta G(^*\mathrm{NH_2}) = 0.53\ \Delta G(^*\mathrm{NOH}) - 1.91;\ R^2 = 0.94 \quad (4)$$

$$\Delta G(^*\mathrm{NH}) = 0.72\ \Delta G(^*\mathrm{N}) - 0.96;\ R^2 = 0.99 \quad (5)$$

$$\Delta G(^*\mathrm{NH_2}) = 0.39\ \Delta G(^*\mathrm{N}) - 1.61;\ R^2 = 0.96 \quad (6)$$

$$\Delta G(^*\mathrm{NH_2}) = 0.55\ \Delta G(^*\mathrm{NH}) - 1.07;\ R^2 = 0.99 \quad (7)$$

It can be observed, for instance, that the correlation observed between *NO and *NOH, eq 1, implies a low free energy cost if the NO species can be stabilized on the metal surface. Similarly, the correlation between *NOH and *N, eq 2, suggests that a greater stabilization of the NOH species on the metal surface will result in a greater liability of the OH moiety to be subsequently released as H_2O after hydrogenation. Ultimately, these correlations establish structure−reactivity relationships where the energetic estimation of certain species allows us to predict the stability of subsequent states.

CONCLUSIONS

The reaction mechanism for NO_x conversion into NH_3, starting from its most oxidized form, NO_2, has been studied by means of plane-wave DFT modeling. To this end, a series of flat surfaces, namely, (110), (111), and (0001), in selected middle-to-late transition metals were used as electrocatalysts, specifically bcc (Fe, Mo), fcc (Ag, Au, Cu, Ir, Ni, Pd, Pt, Rh), and hcp (Co, Os, Ru, Zn) *d*-block metals. Our calculations were performed in aqueous solution via an implicit solvation model, showing free

https://doi.org/10.1021/acs.jpcc.4c08529
J. Phys. Chem. C XXXX, XXX, XXX−XXX

energy results under neutral pH conditions (pH 7) with no applied bias ($U = 0$). The proposed reaction mechanism entailed the addition of seven H^+/e^- pairs in successive elementary reactions divided into two main stages: O-hydrogenation from NO_x, with concomitant formation of water via the path $*NO_2 \rightarrow *NO_2H \rightarrow *NO\ (+H_2O) \rightarrow *NOH \rightarrow *N\ (+H_2O)$, followed by the sequential hydrogenation of N adatoms to form NH_3 via the path $*N \rightarrow *NH \rightarrow *NH_2 \rightarrow *NH_3$.

Our results showed that NO_2 adsorption was spontaneous for all of the metals modeled herein, with maximum stabilization values for middle *d*-block metals (Fe, Mo, Ru, and Os). NO adsorption was also spontaneous, showing binding free energies higher than those computed for NO_2, although they followed a reversed trend with maximum stabilization values for the least electropositive metals (Cu, Zn, Ag, and Au). In general, the hydrogenation of either $*NO_2$ into $*NO_2H$ or *NO into *NOH represented the rate-determining steps of the overall reaction, with the exception of Fe.

Since maximum free energy contributions were less than 1 eV in aqueous solution and neutral pH, the electrocatalytic reduction of NO_x over these metal surfaces is suggested here as a promising process toward environmental applications. To this end, it is particularly interesting to highlight the low overpotentials computed for metals such as Ir or Pt: −0.41 and −0.55 V vs. NHE, respectively, at neutral pH.

Among the most interesting mechanistic aspects of the overall NO_xRR, our results showed that NO_2 adsorption is more exergonic than NH_3 desorption, computing, in most cases, stronger binding free energies for NO_2 and NO than for NH_3, which prevents ammonia poisoning on the metal surfaces. A representation of the formation free energies of all species in the NO_xRR mechanism as a function of atomic number displayed periodic trends following a decreasing ΔG stabilization from medium-to-late *d*-block metals. This periodic behavior was also observed when representing binding free energies of NO_2 reactants and H adatoms (*H) as intermediate species for HER. Thus, the two processes, NO_xRR and HER, seem to be noncompetitive, since both NO_2 and NO adsorption showed greater stabilization, i.e., higher binding free energies, than that computed for the formation of *H species. Additionally, a strong linear correlation has been described among the free energies involving the states *NO vs. *NOH, *NOH vs. N and NH_x (x = 1, 2), *N vs. NH_x (x = 1, 2), and *NH vs. NH_2.

■ ASSOCIATED CONTENT

Supporting Information

The Supporting Information is available free of charge at https://pubs.acs.org/doi/10.1021/acs.jpcc.4c08529.

Full computational details (Section 1) and optimized Cartesian coordinates (Section 2) (PDF)

■ AUTHOR INFORMATION

Corresponding Author

Luis Miguel Azofra − *Instituto de Estudios Ambientales y Recursos Naturales (iUNAT), Universidad de Las Palmas de Gran Canaria (ULPGC), Las Palmas de Gran Canaria 35017, Spain;* orcid.org/0000-0003-4974-1670; Email: luismiguel.azofra@ulpgc.es

Authors

Pilar Carro − *Área de Química Física, Departamento de Química, Facultad de Ciencias, Universidad de La Laguna, Instituto de Materiales y Nanotecnología, La Laguna 3820, Spain;* orcid.org/0000-0001-8073-9857

Raúl Quesada-Cabrera − *Instituto de Estudios Ambientales y Recursos Naturales (iUNAT), Universidad de Las Palmas de Gran Canaria (ULPGC), Las Palmas de Gran Canaria 35017, Spain*

José Miguel Doña-Rodríguez − *Instituto de Estudios Ambientales y Recursos Naturales (iUNAT), Universidad de Las Palmas de Gran Canaria (ULPGC), Las Palmas de Gran Canaria 35017, Spain*

Complete contact information is available at: https://pubs.acs.org/10.1021/acs.jpcc.4c08529

Notes

The authors declare no competing financial interest.

■ ACKNOWLEDGMENTS

L.M.A., R.Q-.C., and J.M.D-.R. are grateful to the Spanish Ministry of Science, Innovation and Universities (Agencia Estatal de Investigación), MCIU/AEI, and Next Generation EU/PRTR programme for financial support (project ref PID2022-143294OB-I00). R.Q-.C. acknowledges the MCIU for his Beatriz Galindo Senior fellowship (ref BG20-00072). L.M.A. acknowledges the MCIU/AEI and NextGenerationEU/PRTR for his Ramón y Cajal fellowship (ref RYC2021-030994-I). L.M.A. is also grateful for access to the KAUST Supercomputer Laboratory (KSL), KSA (Shaheen II and Shaheen III), and Instituto de Astrofísica de Canarias (IAC) for access to LaPalma supercomputer.

■ REFERENCES

(1) MacFarlane, D. R.; Cherepanov, P. V.; Choi, J.; Suryanto, B. H. R.; Hodgetts, R. Y.; Bakker, J. M.; Ferrero Vallana, F. M.; Simonov, A. N. A Roadmap to the Ammonia Economy. *Joule* **2020**, *4*, 1186−1205.

(2) MacFarlane, D. R.; Choi, J.; Suryanto, B. H. R.; Jalili, R.; Chatti, M.; Azofra, L. M.; Simonov, A. N. Liquefied Sunshine—Transforming Renewables into Fertilizers and Energy Carriers with Electromaterials. *Adv. Mater.* **2020**, *32*, No. 1904804.

(3) Suryanto, B. H. R.; Du, H.-L.; Wang, D.; Chen, J.; Simonov, A. N.; MacFarlane, D. R. Challenges and Prospects in the Catalysis of Electroreduction of Nitrogen to Ammonia. *Nat. Catal.* **2019**, *2*, 290−296.

(4) Choi, J.; Suryanto, B. H. R.; Wang, D.; Du, H.-L.; Hodgetts, R. Y.; Ferrero Vallana, F. M.; MacFarlane, D. R.; Simonov, A. N. Identification and Elimination of False Positives in Electrochemical Nitrogen Reduction Studies. *Nat. Commun.* **2020**, *11*, No. 5546.

(5) Andersen, S. Z.; Čolić, V.; Yang, S.; Schwalbe, J. A.; Nielander, A. C.; McEnaney, J. M.; Enemark-Rasmussen, K.; Baker, J. G.; Singh, A. R.; et al. A Rigorous Electrochemical Ammonia Synthesis Protocol with Quantitative Isotope Measurements. *Nature* **2019**, *570*, 504−508.

(6) Martín, A. J.; Veenstra, F. L. P.; Lüthi, J.; Verel, R.; Pérez-Ramírez, J. Toward Reliable and Accessible Ammonia Quantification in the Electrocatalytic Reduction of Nitrogen. *Chem. Catal.* **2021**, *1*, 1505−1518.

(7) Carro, P.; Choi, J.; MacFarlane, D.; Simonov, A. N.; Doña-Rodriguez, J. M.; Azofra, L. M. Competition between Metal-Catalysed Electroreduction of Dinitrogen, Protons, and Nitrogen Oxides: A DFT Perspective. *Catal. Sci. Technol.* **2022**, *12*, 2856−2864.

(8) Long, J.; Chen, S.; Zhang, Y.; Guo, C.; Fu, X.; Deng, D.; Xiao, J. Direct Electrochemical Ammonia Synthesis from Nitric Oxide. *Angew. Chem., Int. Ed.* **2020**, *59*, 9711−9718.

(9) Ko, B. H.; Hasa, B.; Shin, H.; Zhao, Y.; Jiao, F. Electrochemical Reduction of Gaseous Nitrogen Oxides on Transition Metals at Ambient Conditions. *J. Am. Chem. Soc.* **2022**, *144*, 1258−1266.

(10) Wang, D.; Chen, Z.-W.; Gu, K.; Chen, C.; Liu, Y.; Wei, X.; Singh, C. V.; Wang, S. Hexagonal Cobalt Nanosheets for High-Performance Electrocatalytic NO Reduction to NH_3. *J. Am. Chem. Soc.* **2023**, *145*, 6899−6904.
(11) Li, Y.; Cheng, C.; Han, S.; Huang, Y.; Du, X.; Zhang, B.; Yu, Y. Electrocatalytic Reduction of Low-Concentration Nitric Oxide into Ammonia over Ru Nanosheets. *ACS Energy Lett.* **2022**, *7*, 1187−1194.
(12) Shao, J.; Jing, H.; Wei, P.; Fu, X.; Pang, L.; Song, Y.; Ye, K.; Li, M.; Jiang, L.; Ma, J.; et al. Electrochemical Synthesis of Ammonia from Nitric Oxide Using a Copper−Tin Alloy Catalyst. *Nat. Energy* **2023**, *8*, 1273−1283.
(13) Chen, K.; Wang, F.; Lu, X.; Li, Y.; Chu, K. Atomically Dispersed W_1−O_3 Bonded on Pd Metallene for Cascade NO Electroreduction to NH_3. *ACS Catal.* **2023**, *13*, 9550−9557.
(14) Chen, K.; Xiang, J.; Guo, Y.; Liu, X.; Li, X.; Chu, K. Pd_1Cu Single-Atom Alloys for High-Current-Density and Durable NO-to-NH_3 Electroreduction. *Nano Lett.* **2024**, *24*, 541−548.
(15) Li, X.; Chen, K.; Lu, X.; Ma, D.; Chu, K. Atomically Dispersed Co Catalyst for Electrocatalytic NO Reduction to NH_3. *Chem. Eng. J.* **2023**, *454*, No. 140333.
(16) Chen, K.; Zhang, G.; Li, X.; Zhao, X.; Chu, K. Electrochemical NO Reduction to NH_3 on Cu Single Atom Catalyst. *Nano Res.* **2023**, *16*, 5857−5863.
(17) Chen, K.; Wang, J.; Zhang, H.; Ma, D.; Chu, K. Self-Tandem Electrocatalytic NO Reduction to NH_3 on a W Single-Atom Catalyst. *Nano Lett.* **2023**, *23*, 1735−1742.
(18) Chen, K.; Wang, G.; Guo, Y.; Ma, D.; Chu, K. Iridium Single-Atom Catalyst for Highly Efficient NO Electroreduction to NH_3. *Nano Res.* **2023**, *16*, 8737−8742.
(19) Chen, K.; Zhang, Y.; Xiang, J.; Zhao, X.; Li, X.; Chu, K. P-Block Antimony Single-Atom Catalysts for Nitric Oxide Electroreduction to Ammonia. *ACS Energy Lett.* **2023**, *8*, 1281−1288.
(20) Chen, K.; Zhang, N.; Wang, F.; Kang, J.; Chu, K. Main-Group Indium Single-Atom Catalysts for Electrocatalytic NO Reduction to NH_3. *J. Mater. Chem. A* **2023**, *11*, 6814−6819.
(21) Lin, Y.; Liang, J.; Li, H.; Zhang, L.; Mou, T.; Li, T.; Yue, L.; Ji, Y.; Liu, Q.; Luo, Y.; et al. Bi Nanodendrites for Highly Efficient Electrocatalytic NO Reduction to NH_3 at Ambient Conditions. *Matert. Today Phys.* **2022**, *22*, No. 100611.
(22) Li, Z.; Ma, Z.; Liang, J.; Ren, Y.; Li, T.; Xu, S.; Liu, Q.; Li, N.; Tang, B.; Liu, Y.; et al. MnO_2 Nanoarray with Oxygen Vacancies: An Efficient Catalyst for NO Electroreduction to NH_3 at Ambient Conditions. *Mater. Today Phys.* **2022**, *22*, No. 100586.
(23) Li, Z.; Zhou, Q.; Liang, J.; Zhang, L.; Fan, X.; Zhao, D.; Cai, Z.; Li, J.; Zheng, D.; He, X.; et al. Defective TiO_{2-x} for High-Performance Electrocatalytic NO Reduction toward Ambient NH_3 Production. *Small* **2023**, *19*, No. 2300291.
(24) Liang, J.; Liu, P.; Li, Q.; Li, T.; Yue, L.; Luo, Y.; Liu, Q.; Li, N.; Tang, B.; Alshehri, A. A.; et al. Amorphous Boron Carbide on Titanium Dioxide Nanobelt Arrays for High-Efficiency Electrocatalytic NO Reduction to NH_3. *Angew. Chem., Int. Ed.* **2022**, *61*, No. e202202087.
(25) Chen, K.; Shen, P.; Zhang, N.; Ma, D.; Chu, K. Electrocatalytic NO Reduction to NH_3 on Mo_2C Nanosheets. *Inorg. Chem.* **2023**, *62*, 653−658.
(26) Zhang, L.; Liang, J.; Wang, Y.; Mou, T.; Lin, Y.; Yue, L.; Li, T.; Liu, Q.; Luo, Y.; Li, N.; et al. High-Performance Electrochemical NO Reduction into NH_3 by MoS_2 Nanosheet. *Angew. Chem., Int. Ed.* **2021**, *60*, 25263−25268.
(27) Mou, T.; Liang, J.; Ma, Z.; Zhang, L.; Lin, Y.; Li, T.; Liu, Q.; Luo, Y.; Liu, Y.; Gao, S.; et al. High-Efficiency Electrohydrogenation of Nitric Oxide to Ammonia on a Ni_2P Nanoarray under Ambient Conditions. *J. Mater. Chem. A* **2021**, *9*, 24268−24275.
(28) Lim, J.; Fernández, C. A.; Lee, S. W.; Hatzell, M. C. Ammonia and Nitric Acid Demands for Fertilizer Use in 2050. *ACS Energy Lett.* **2021**, *6*, 3676−3685.
(29) Cardoso, J. S.; Silva, V.; Rocha, R. C.; Hall, M. J.; Costa, M.; Eusébio, D. Ammonia as an Energy Vector: Current and Future Prospects for Low-Carbon Fuel Applications in Internal Combustion Engines. *J. Clean Prod.* **2021**, *296*, No. 126562.
(30) Kumar, A.; Vibhu, V.; Bassat, J.-M.; Nohl, L.; de Haart, L. G. J. Bert.; Bouvet, M.; Eichel, R.-A. Ammonia as a Potential Energy Vector in the Burgeoning Hydrogen Economy. *ChemElectroChem.* **2024**, *11*, No. e202300845.
(31) Rhimi, B.; Padervand, M.; Jouini, H.; Ghasemi, S.; Bahnemann, D. W.; Wang, C. Recent Progress in NO_x Photocatalytic Removal: Surface/Interface Engineering and Mechanistic Understanding. *J. Environ. Chem. Eng.* **2022**, *10*, No. 108566.
(32) Hammer, B.; Hansen, L. B.; Nørskov, J. K. Improved Adsorption Energetics within Density-Functional Theory Using Revised Perdew-Burke-Ernzerhof Functionals. *Phys. Rev. B* **1999**, *59*, 7413−7421.
(33) Monkhorst, H. J.; Pack, J. D. Special Points for Brillouin-Zone Integrations. *Phys. Rev. B* **1976**, *13*, 5188−5192.
(34) Grimme, S.; Antony, J.; Ehrlich, S.; Krieg, H. A Consistent and Accurate Ab Initio Parametrization of Density Functional Dispersion Correction (DFT-D) for the 94 Elements H-Pu. *J. Chem. Phys.* **2010**, *132*, No. 154104.
(35) Grimme, S.; Ehrlich, S.; Goerigk, L. Effect of the Damping Function in Dispersion Corrected Density Functional Theory. *J. Comput. Chem.* **2011**, *32*, 1456−1465.
(36) Mathew, K.; Sundararaman, R.; Letchworth-Weaver, K.; Arias, T. A.; Hennig, R. G. Implicit Solvation Model for Density-Functional Study of Nanocrystal Surfaces and Reaction Pathways. *J. Chem. Phys.* **2014**, *140*, No. 84106.
(37) Mathew, K.; Kolluru, V. S. C.; Mula, S.; Steinmann, S. N.; Hennig, R. G. Implicit Self-Consistent Electrolyte Model in Plane-Wave Density-Functional Theory. *J. Chem. Phys.* **2019**, *151*, No. 234101.
(38) Kresse, G.; Hafner, J. Ab Initio Molecular Dynamics for Liquid Metals. *Phys. Rev. B* **1993**, *47*, 558−561.
(39) Kresse, G.; Hafner, J. Ab Initio Molecular-Dynamics Simulation of the Liquid-Metal–Amorphous-Semiconductor Transition in Germanium. *Phys. Rev. B* **1994**, *49*, 14251−14269.
(40) Kresse, G.; Furthmüller, J. Efficient Iterative Schemes for Ab Initio Total-Energy Calculations Using a Plane-Wave Basis Set. *Phys. Rev. B* **1996**, *54*, 11169−11186.
(41) Kresse, G.; Furthmüller, J. Efficiency of Ab-Initio Total Energy Calculations for Metals and Semiconductors Using a Plane-Wave Basis Set. *Comput. Mater. Sci.* **1996**, *6*, 15−50.
(42) Liu, H.; Bai, L.; Bergmann, A.; Cuenya, B. R.; Luo, J. Electrocatalytic Reduction of Nitrogen Oxide Species to Ammonia. *Chem.* **2024**, *10*, 2963−2986.
(43) Wang, F.; Shang, S.; Sun, Z.; Yang, X.; Chu, K. Electrocatalytic Nitrite Reduction to Ammonia on In_1Cu Single Atom Alloy. *Chem. Eng. J.* **2024**, *489*, No. 151410.
(44) Yin, H.; Du, A. Emerging Role of *p*-Block Element in Catalyzing Electrochemical NO_x Reduction to Ammonia: A Theoretical Perspective. *Adv. Funct. Mater.* **2024**, *34*, No. 2403718.
(45) Xie, M.; Tang, S.; Li, Z.; Wang, M.; Jin, Z.; Li, P.; Zhan, X.; Zhou, H.; Yu, G. Intermetallic Single-Atom Alloy In−Pd Bimetallene for Neutral Electrosynthesis of Ammonia from Nitrate. *J. Am. Chem. Soc.* **2023**, *145*, 13957−13967.
(46) Azofra, L. M. Nitrogen Reduction Reaction (NRR) Modelling: A Case That Illustrates the Challenges of DFT Studies in Electrocatalysis. *Curr. Opin. Electrochem.* **2022**, *35*, No. 101073.
(47) Höskuldsson, Á. B.; Sakai, Y.; Skúlason, E. Modeling Electrochemical Nitrogen Reduction. *Chem. Catal.* **2025**, *5*, No. 101239.

https://doi.org/10.1021/acs.jpcc.4c08529
J. Phys. Chem. C XXXX, XXX, XXX−XXX